A New Condensed Gas Calorimeter. Thermodynamic Properties of Solid and Liquid Dinitrogen Oxide

Tooru ATAKE and Hideaki CHIHARA

Department of Chemistry, Faculty of Science, Osaka University, Toyonaka 560

(Received June 3, 1974)

A new adiabatic calorimeter for use with condensed gases from 1.8 K to room temperature has been constructed. The heat capacity of solid and liquid dinitrogen oxide was measured between 1.9 and 184 K together with the vapor pressure above 146 K. The residual entropy was re-evaluated as 6.0 J K^{-1} mol^{-1}, which is now closer to R ln2, suggesting that the disorder of molecular end-for-end orientation is perfectly frozen in the solid state. The moments of lattice frequency spectrum were derived from low-temperature heat capacities and high-temperature vapor pressures. The anomalous increase of heat capacity below the triple point was interpreted as arising from thermal creation of orientational defects with the enthalpy of formation 10.8 kJ mol^{-1}. Other thermodynamic quantities determined are as follows: triple point of pure N_2O 182.407±0.002 K, heat of fusion 6 516±20 J mol^{-1}, entropy of fusion 35.7±0.1 J K^{-1} mol^{-1}, heat of vaporization at 184.81 K and 101.7 kPa 16 544± 20 J mol^{-1}, normal boiling point 184.74 K, translational zero-point energy 1.6±0.3 kJ mol^{-1}, Debye temperature corresponding to $3N$ degrees of freedom 141.0±1.0 K.

Dynamical properties of molecules in the solid state has attracted attention from experimental as well as theoretical points of view. Crystals of monatomic molecules have been studied by a variety of methods and their properties are rather well understood. The crystals of linear molecules have librational degrees of freedom which add some complexity to what has been known for monatomic crystals. In particular, α-CO and N_2O crystallize in a modified fcc lattice in which a molecular axis is oriented along one of the body diagonals in such a way that molecular quadrupole interaction determines the arrangement. Furthermore, there is a possibility of head-to-tail disorder, which has been considered to be at least partially frozen-in at low temperatures, as inferred from the existence of the residual entropy ($\approx R \ln 2$) determined by Giauque *et al.*[1,2] In 1964, however, Melhuish and Scott[3] calculated the Curie temperatures for the order-disorder transitions associated with molecular reorientation in solid CO and N_2O from evaluation of electrostatic energies, and they suggested that the transitions were to be expected at 5 and 11 K, respectively. Because these transition points were lower than the lowest temperature (about 15 K) from which Giauque *et al.*[1,2] started measurements of the heat capacities, attempts were made to locate the transition by extending the measurements on carbon monoxide to lower temperatures (down to 2.5 K) by the authors and J. A. Morrison and their coworkers in 1966.[4,5] Although no additional phase transition was found, the residual entropy of carbon monoxide was re-evaluated as 3.3±0.8 J K^{-1} mol^{-1}, which was significantly different from the value of $R \ln 2 = 5.76$ J K^{-1} mol^{-1}. In 1968, Pitzer *et al.*[6] examined kinetics of the order-disorder transition by tunneling mechanism and found the rate of transition to be unobservably slow. In 1969, Burford and Graham[7] further extended the heat capacity measurements on carbon monoxide down to about 0.8 K but failed to find an anomaly. For decisive explanation of the residual entropy of solid carbon monoxide, therefore, more investigation is still required. In the case of dinitrogen oxide, which is analogous to carbon monoxide in many respects, the calculated Curie temperature for the order-disorder transition is higher by a factor of 2. Therefore, more precise calorimetry below 15 K seemed to be in order. This paper reports the measurements of heat capacity and related thermodynamic properties of dinitrogen oxide and the results are analyzed in detail. In the course of this investigation, we found unusually large 'premelting' tail of the heat capacity below the triple point, which will be interpreted in terms of defect formation in the solid.

Descriptions will be presented of the new adiabatic calorimeter for use with condensed gases which works between 1.8 K and room temperature. Some modifications and improvements of the measuring system over the earlier model[4,8] will also be described.

Experimental

Calorimeter and Cryostat. A cryostat and an adiabatic calorimeter for condensed gases have been newly designed and constructed. The sectional plan of the apparatus is shown in Fig. 1. A feature of the cryostat is that it has two refrigerant containers of cascade type E, (inside volume of 430 cm^3) and I (1 770 cm^3), above the calorimeter vessel A, the adiabatic mantle B and the thermal sink C. The two containers are made of heavy brass and may be loaded with different refrigerants depending on the temperature region to work with. For the measurements from 2.6 to 13 K, the container E is filled with liquid helium which, by a single charging, lasts about twenty hours, as long as there is solid hydrogen in the container I. For the measurements in the lowest temperature region down to 1.8 K, both containers are filled with liquid helium in which case the refrigerant lasts about ten hours. The inner jacket H is soldered vacuum-tight to the hydrogen container I with Wood's alloy but the radiation shield D is only thermally anchored to the container E because the space inside H is a common vacuum. Both H and D are made of copper whereas the outer jacket J is made of brass. All the tubes a—f are made of SUS-27 stainless steel and have outside diameters of 10—16 mm and wall thickenss of 0.15 mm. The entire cryostat can be evacuated through the tubes c and f and maintained in a vacuum better than 1×10^{-4} Pa during measurements. The calorimeter is cooled by breaking the vacuum with small amount of helium exchange gas down to about 15 K. Below

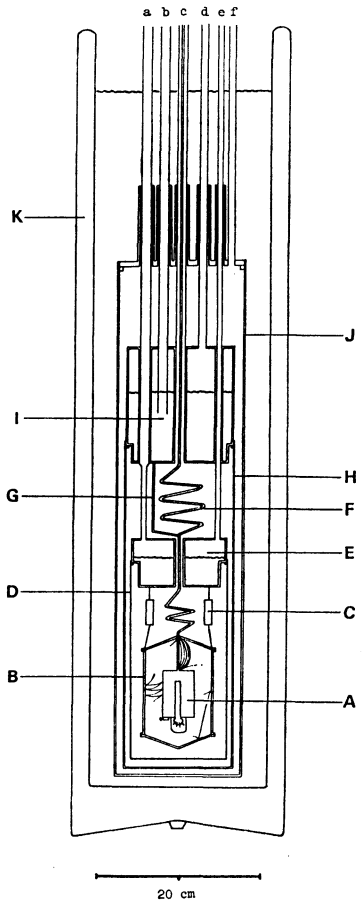

Fig. 1. The calorimeter assembly. A, Calorimeter vessel; B, Adiabatic mantle; C, Thermal sink; D, Radiation shield; E, Refrigerant container; F, Sample filling tube; G, Thermal shunt; H, Inner jacket; I, Refrigerant container; J, Outer jacket; K, Liquid nitrogen Dewar; a and b, Refrigerant transfer tubes; c, Inner jacket evacuation tube; d and e, Refrigerant evacuation tubes; f, Outer jacket evacuation tube.

about 15 K, the calorimeter is cooled only by heat conduction through the electrical leads. The sample filling tube F (German silver, 1 mm in outside diameter, 0.1 mm in wall thickness, 163 cm in length) connects the calorimeter vessel A to the external gas handling system (see Fig. 3). The filling tube is thermally anchored to the bottom of the container I by way of a short insert of copper wire (G in Fig. 1), over the length of which a Manganin heater is wound to prevent the gas from condensing at the cold spot. This thermal shunt is used when measurements are made in the lowest temperature region, where the sample has negligible vapor pressures, to keep minimum the heat leak into the calorimeter through the tube. Manganin heaters (B.S. # 36) are also closely wound non-inductively over the entire length of the filling tube except the portions inside the mantle B and above the top of the cryostat, and the heater wires are varnished to the tube with glyptal lacquer (G.E. adhesive No. 7031). The heaters are wound in seven separate parts and the temperature of each part is monitored and measured with a Constantan *vs.* Chromel-P thermocouple. Four lower parts of the filling tube may be at so low a temperature that a thermocopule would not have a sufficient sensitivity and therefore the parts are also equipped with carbon resistors (nominal value of 10 Ω, Allen-Bradley Co.) to use in the

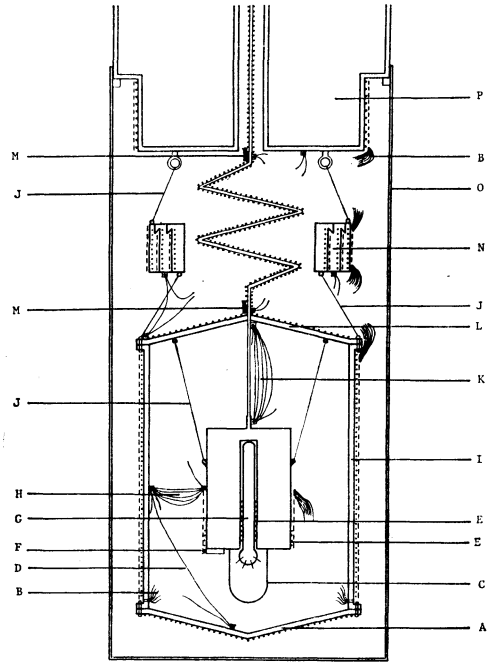

Fig. 2. The lower part of the cryostat. ------, Lead wires; ·····, Heater wires; A, Adiabatic mantle (Bottom); B, Lead wires; C, Radiation shield; D, Difference thermocouple between side and bottom; E, Calorimeter heater; F, Germanium thermometer; G, Platinum thermometer; H, Difference thermocouple between side and calorimeter; I, Adiabatic mantle (Side); J, Nylon cord; K, Difference thermocouple between top and calorimeter; L, Adiabatic mantle (Top); M, Carbon thermometer and thermocouple; N, Thermal sink; O, Radiation shield; P, Refrigerant container.

low temperature region. The electrical leads are double silk-insulated B.S. # 36 copper and are in good thermal contact with the refrigerant containers I and E at their bottoms.

Figure 2 shows the lower part of the cryostat. The copper thermal sink N is of three year-ring shaped construction for securing good thermal contact between the wires and the rings. The calorimeter vessel (gold, 44 cm^3 in volume, 75 g in net weight) has eight vanes for the inside thermal uniformity. A platinum resistance thermometer G is cast into the reentrant well with Wood's alloy and a germanium resistance thermometer F is fitted into a copper sheath which is soldered to the bottom of the vessel. The calorimeter heater E (150 Ω, B.S. # 36 KARMA wire, Driver-Harris Co.) is wound around the lower part of the vessel and also around the lower part of the platinum thermometer. The copper adiabatic mantle consists of three parts whose temperatures are monitored and controlled separately as described in the earlier paper.[8] The filling tube from the calorimeter vessel is soldered to the top L to ensure good control of its temperature. All the electrical leads between the calorimeter vessel and the terminal box outside the cryostat have soldered connections only at the bottom of the side of the mantle I.

External Equipments for Gas Handling. The gas handling apparatus external to the cryostat is schematically shown in Fig. 3. It consists of three manometers, a calibrated flask of about 5 dm^3 capacity, and traps for sample distillation. The sample gas from a cylinder or a sealed flask is desiccated

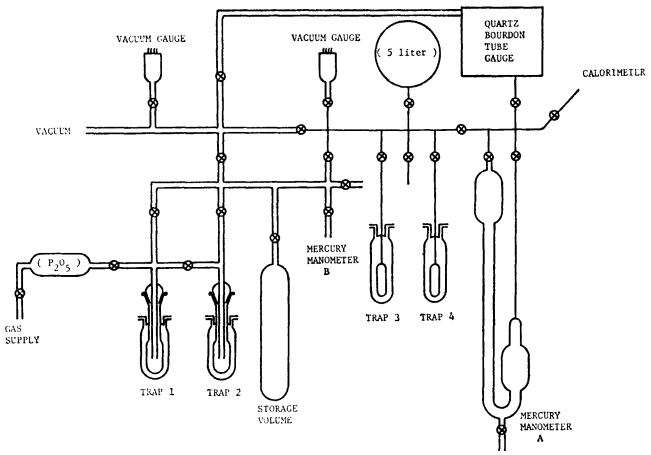

Fig. 3. The gas handling apparatus.

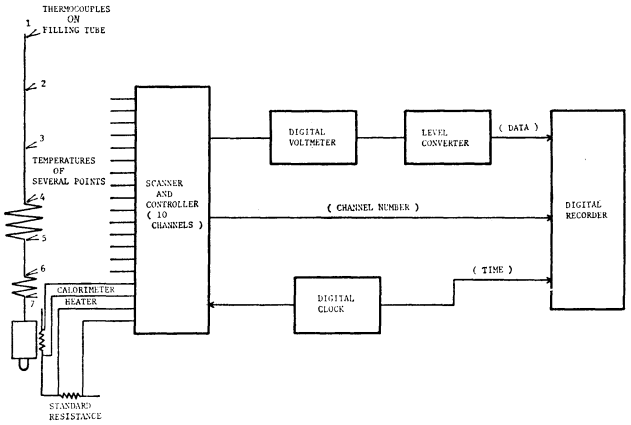

Fig. 4. The data acquisition system.

over P_2O_5 or other desiccants before condensing in trap 1 or 2. The traps 1 and 2 are used for purification by distilling the gas back and forth between the two. The pressure during the distillation is monitored with the mercury manometer B. The gas is then transferred to either trap 3 or 4 depending on the amount of the sample gas. The traps are of special design with a buffer space surrounding the sample container. This space is useful for a fine control of the temperature: a low-melting liquid may be put into this space while the entire trap is immersed in liquid nitrogen or in a cooled empty Dewar vessel (not shown). The condensed gas in trap 3 or 4 is then slowly evaporated into the 5 dm^3 flask (thermostated) and after standing for a sufficient length of time the pressure of the gas is carefully determined with the manometer A or with the quartz Bourdon gage (Texas Instruments Inc., Model 144-01). The dead space volume was determined by using helium as the working gas in advance. The amount of the specimen used for calorimetry is derived from two determinations of the gas before and after the filling into the calorimeter vessel. A small amount of the gas can be taken out into an appendix tube (not shown) for analysis.

In the earlier stage of the present study, the pressure was read on the mercury manometer A and in the later stage, it was determined with the Bourdon gage. The mercury manometer is so designed that it requires no corrections for the capillary depression and causes only small change in the dead space volume. The precision of the manometer is limited to ± 7 Pa, determined by the precision of the standard scale (stainless steel) and of the verniers of the travelling telescopes. The Bourdon gage, on the other hand, has an advantage that the measured volume can be kept constant. This is particularly helpful when measuring the vapor pressures and the heat capacities at the same time.

When measuring heat of vaporization, the calibrated flask is also used as a storage volume of the gas evaporated from the calorimeter vessel. During heat input, the pressure is controlled manually to within ± 150 Pa by adjusting a stopcock, being monitored with the Bourdon gage.

Electrical Measurements. The outputs from the seven thermocouples for measuring the temperature gradient along the length of the filling tube and also the potential and the current across the calorimeter heater are recorded on the automatic data acquisition system, the block diagram of which is shown in Fig. 4. The system consists of a scanner (TR-7216-20S and TR-7513, Takeda Riken Industry Co., Ltd.), a digital integrated voltmeter (3450A, Hewlett-Packard), a digital clock (TR-7414), and a digital printer (TR-6196) which records the time, the channel number, and the outputs of the digital voltmeter. The nominal sensitivity is better than ± 1 μV on the 100 mV range. The method of temperature measurements with platinum and germanium resistance thermometers is the same as that described in the earlier papers.[4,8,9]

Temperature Scales. The platinum resistance thermometer for the present calorimeter (Model 8164, Leeds & Northrup Co.) is the one calibrated on the IPTS-48 and the NBS-55 temperature scales at the U.S. National Bureau of Standards. Therefore, the temperature scale has been converted to the IPTS-68 by using the NEAC-2200-500 computer system at Computer Center of Osaka University.

The germanium scale (used below 13.81 K) was fixed by using a different method for each of the three temperature regions: (a) the 1958 ^{4}He vapor pressure temperature scale below 4.2 K, (b) the ^{4}He gas thermometric temperature scale between 4.2 and 13.81 K (for this purpose the calorimeter was used as a gas thermometer), (c) the IPTS-68 above 13.81 K (the germanium thermometer was compared with the platinum thermometer). The germanium resistance thermometer used in the early stage of this investigation bears the laboratory designation, the germanium thermometer α, and the one used in the later stage the germanium thermometer γ. The germanium thermometer γ (CR-1000, Cryocal Inc.) is of better quality (smaller size and higher sensitivity) than the α (MHSP-2401, Minneapolis-Honeywell Regulator Co.). The following two functions were examined for computer fitting by the method of least squares,

$$\log_{10} R = \sum_{i=1}^{b} A_i T^{i-a}, \tag{1}$$

$$\log_{10} R = \sum_{i=1}^{b} A_i (\log_{10} T)^{i-a}, \tag{2}$$

where R is the resistance in ohm and A_i's are constants. The best fit for germanium thermometer α was obtained by employing the formula:

$$\log_{10} R = \sum_{i=1}^{10} A_i T^{i-2}. \tag{3}$$

The ten coefficients are listed in Table 1, together with the sum of deviations, and the deviation plot is given in Fig. 5. In the second series of the heat capacity measurements of dinitrogen oxide, the α has been replaced by the germanium thermometer γ, which was calibrated by comparison with the resistance of the α. However, below 4.2 K the γ was recalibrated on the 1958 ^{4}He vapor pressure temperature scale, and for this purpose this condensed gas calorimeter was used as a vapor pressure thermometer. In this case, the formula

Table 1. The ten coefficients for the germanium resistance thermometer α.[a,b]

i	A_i	i	A_i
1	−0.072 215 608 7	6	0.028 195 779 8
2	6.182 766 499 5	7	−0.002 509 593 5
3	−2.434 412 857 7	8	0.000 137 184 0
4	0.884 287 351 4	9	−0.000 004 205 8
5	−0.199 832 886 2	10	0.000 000 055 3

a) Calibration formula:
$\log_{10} R=\sum_{i=1}^{10} A_i\ T^{i-2}$

b) Sum of deviations of the 27 calibration points:
$\sum_{i=1}^{27}(\log_{10} R_i(\text{calcd})-\log_{10} R_i(\text{obsd}))^2=0.000\,428\,87$

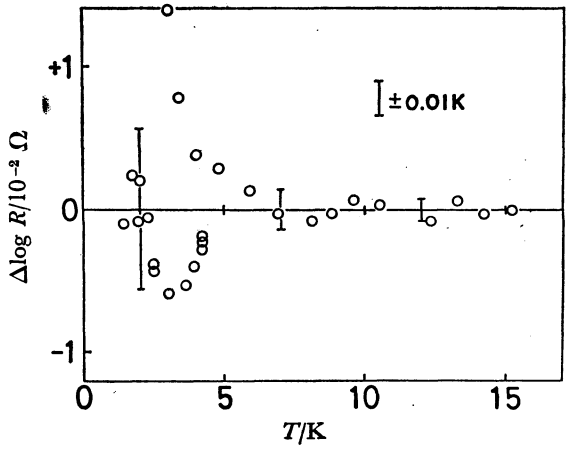

Fig. 5. The deviation plot for the germanium thermometer α fitted to the formula: $\log_{10} R=\sum_{i=1}^{10} A_i \cdot T^{i-2}$.

best fit between 1.7 and 15 K was determined as

$$\log_{10} R = \sum_{i=1}^{10} A_i T^{i-4}. \quad (4)$$

The ten coeffiecients and the sum of deviations are given in Table 2, and the deviation plot is shown in Fig. 6. Apparently, the γ scale is much closer to the measured calibration points than the α scale. Below 4.2 K, especially, the γ scale is more accurate than the α scale.

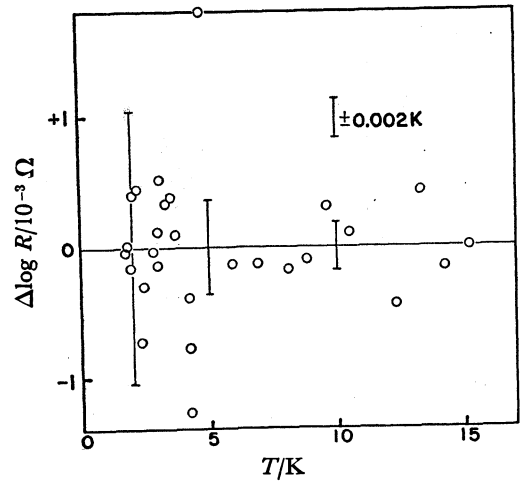

Fig. 6. The deviation plot for the germanium thermometer γ fitted to the formula: $\log_{10} R=\sum_{i=1}^{10} A_i\ T^{i-4}$.

Table 2. The ten coefficients for the germanium resistance thermometer γ.[a,b]

i	A_i	i	A_i
1	−9.904 502 823 5	6	0.341 814 300 2
2	19.518 944 667 3	7	−0.037 495 567 9
3	−14.398 844 122 6	8	0.002 528 407 9
4	10.255 492 344 7	9	−0.000 093 484 3
5	−2.093 324 956 6	10	0.000 001 443 3

a) Calibration formula:
$\log_{10} R=\sum_{i=1}^{10} A_i\ T^{i-4}$

b) Sum of deviations of the 28 calibration points:
$\sum_{i=1}^{28}(\log_{10} R_i(\text{calcd})-\log_{10} R_i(\text{obsd}))^2=0.000\,007\,91$

Material. The sample of dinitrogen oxide in 1 liter flasks at 101 kPa was purchased from Takachiho Kagaku Kogyo Co., Ltd., and its stated purity was 99.9 mol%. Dried over P_2O_5, the dinitrogen oxide was distilled twice by means of the traps 1—4 in Fig. 3. The final purity was 99.999 mol% as determined by the fractional melting method during the calorimetry. Gas-chromatographic and mass-spectrographic analyses showed no detectable impurities. The quantities of the purified dinitrogen oxide used for the calorimetry were determined by the *P-V-T* measurements, corrected for non-ideality of the gas by using published values of the second virial coefficients:[10] 0.426 5±0.001 6 mol in the first series and 0.180 0±0.003 0 mol in the second series. In the second series, however, the runs 1 and 2 were carried out on the sample of the amount of 0.200 7±0.000 5 mol.

Calorimetry. In the first series of the calorimetry on dinitrogen oxide, the germanium thermometer α was used and the pressure was measured with the mercury manometer, which caused the rather large uncertainties of the present results. In the second series, the germanium thermometer γ was used and the pressure was measured with the quartz Bourdon gage.

At high temperatures, the filling tube temperatures were so adjusted that the calorimeter may be the coldest in order to prevent distillation of the specimen out of the calorimeter.

No helium gas was introduced into the calorimeter vessel for heat exchange. The time for thermal equilibrium within the calorimeter vessel was a few seconds in the lowest temperature region, one minute at about 20 K, and a few minutes at about 50 K, increasing to ten or more minutes above 100 K.

In the region below about 10 K, the adiabatic condition between the calorimeter and the mantle was controlled manually because the sensitivity of the thermocopules was not sufficient to energize the automatic control device.[8]

Results

Heat Capacity. The heat capacity of dinitrogen oxide was measured between 1.9 and 184 K. The temperature rise by a single heat input was 0.3—0.5 K below 10 K, about 1 K below 30 K, and about 2 K above 30 K. Because the liquid phase exists over only 2.4 K temperature interval, a single temperature rise was chosen as about 1 K in this region. Corrections to the heat capacity were necessary above 140 K for vaporization of the solid or the liquid and other accompanying effects. Other quantities relevant for heat capacity computation were evaluated in the following

TABLE 3. HEAT CAPACITY OF DINITROGEN OXIDE
1 mol N_2O=44.012 8 g, IPTS-68

T/K	C_p/J K^{-1} mol^{-1}
Series I	
(Run 1)	
2.676	0.014 2
3.002	0.020 5
3.414	0.029 9
3.824	0.041 4
4.260	0.057 5
4.755	0.078 8
5.306	0.108 2
5.881	0.148 4
6.437	0.195 8
6.969	0.252 3
7.454	0.314 8
7.887	0.380 1
8.315	0.448 0
8.768	0.534 1
9.261	0.635 0
9.787	0.765 3
10.352	0.924 3
10.979	1.113 0
11.650	1.329 4
(Run 2)	
2.935	0.018 9
3.355	0.027 9
3.762	0.038 8
4.202	0.054 2
4.688	0.072 3
5.173	0.098 5
5.650	0.129 2
6.110	0.163 8
6.567	0.207 4
7.028	0.258 7
7.481	0.317 0
7.920	0.381 0
8.353	0.451 5
8.802	0.536 1
9.274	0.638 6
9.775	0.764 5
10.329	0.905 7
(Run 3)	
3.017	0.020 9
3.447	0.030 2
(Run 4)	
3.078	0.021 5
3.487	0.032 6
3.895	0.043 8
4.339	0.058 3
(Run 5)	
11.582	1.306 2
12.105	1.511 4
12.725	1.766
13.342	2.054
13.970	2.343
(Run 6)	
11.647	1.336 2
12.257	1.578 9
12.871	1.830
13.491	2.121
14.125	2.431
14.795	2.800
15.509	3.221
16.290	3.682
17.163	4.275
18.130	4.936
19.215	5.720
20.305	6.544
21.272	7.299
22.148	8.000
(Run 7)	
11.675	1.354 7
12.374	1.629 5
13.062	1.922
13.755	2.261
14.467	2.624
15.203	3.040
15.957	3.490
16.744	3.984
17.650	4.605
18.650	5.309
19.658	6.045
(Run 8)	
20.886	7.006
21.911	7.817
22.948	8.654
24.011	9.519
25.114	10.424
26.356	11.437
27.718	12.563
29.064	13.655
30.374	14.701
31.731	15.78
33.133	16.85
34.491	17.88
35.824	18.84
(Run 9)	
30.436	14.74
31.997	15.97
33.524	17.13
35.033	18.24
36.537	19.32
38.152	20.43
39.866	21.57
41.598	22.65
43.378	23.71
45.198	24.75
47.069	25.77
49.003	26.77
51.050	27.79
52.018	28.16
(Run 10)	
50.375	27.41
52.383	28.35
54.468	29.28
56.481	30.11
58.433	30.87
60.332	31.59
61.769	32.11
63.471	32.68
65.184	33.23
66.894	33.74
68.604	34.25
70.316	34.72
72.047	35.22
73.815	35.69
75.625	36.16
77.478	36.62
79.358	37.09
81.249	37.52
83.134	37.94
(Run 11)	
82.159	37.71
84.241	38.19
86.295	38.62
88.321	39.07
90.322	39.47
92.301	39.86
94.260	40.19
96.195	40.61
98.111	41.03
(Run 12)	
96.473	40.62
98.436	40.98
100.419	41.36
102.404	41.66
104.372	42.01
106.325	42.42
108.274	42.81
110.225	43.22
112.159	43.54
114.080	43.85
116.005	44.20
117.936	44.52
(Run 13)	
118.749	44.57
120.936	44.83
123.228	45.44
125.873	45.92
128.812	46.53
131.789	47.04
134.878	47.64
138.008	48.25
141.181	48.87
144.437	49.55
(Run 14)	
147.686	50.19
150.933	50.93
154.174	51.67
157.408	52.38
160.634	53.19
163.841	53.99
167.025	54.85
170.194	55.46
172.864	56.27
175.018	56.85
177.132	57.57
179.199	58.14
181.097	58.74
(fusion)	
183.215	76.79
184.241	77.43
(Run 15)	
183.096	76.45
183.993	76.46
Series II	
(Run 1)	
72.756	35.37
74.656	35.90
76.611	36.39
78.563	36.93
80.517	37.32
82.485	37.82
84.448	38.28
86.560	38.75
88.823	39.18
(Run 2)	
163.421	53.62
167.246	54.58
171.131	55.63
174.742	56.56
177.929	57.58
180.558	58.29
(fusion)	
183.062	76.19
(Run 3)	
1.907	0.004 6
2.193	0.007 7
2.570	0.010 9
2.988	0.018 2
3.400	0.026 2
3.830	0.038 2
4.248	0.053 5
4.655	0.069 3
(Run 4)	
3.453	0.027 9
3.957	0.043 0
4.491	0.062 2
5.009	0.087 3
(Run 5)	
184.427	78.00

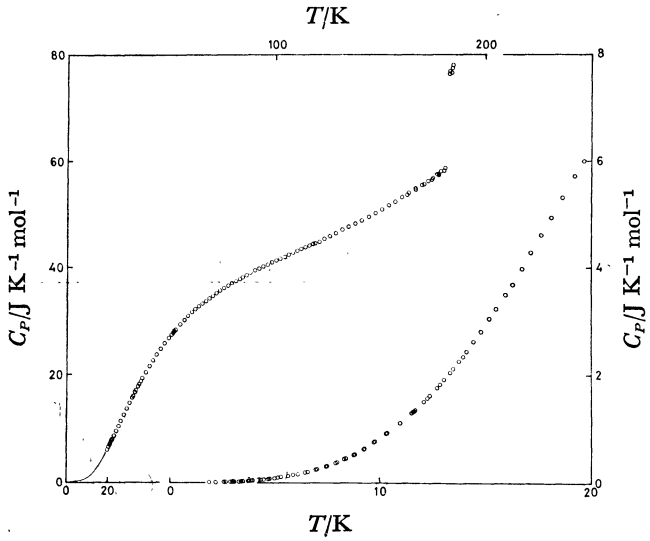

Fig. 7. Molar heat capacity of dinitrogen oxide.

way. The density of solid N_2O has been reported only at two temperatures (molar volume 27.0 cm^3 at 20 K and lattice constant a_0=0.566 nm at −190 °C);[11,12] therefore the densities at other temperatures were estimated by linear extrapolation to higher temperatures. The liquid densities were obtained by smoothing the published data.[13] The heat capacity of the gas of dinitrogen oxide was calculated from the spectroscopic data: fundamental frequencies of 1 277 cm^{-1}, 589 cm^{-1} (doubly degenerate) and 2 224 cm^{-1}. The values of the second virial coefficient were taken from literature;[10] however, they had to be extrapolated to below 197 K. The overall correction amounted to at most about 5% of the total input energy. In the first series of measurements, the calorimeter vessel contributed about 40% of the total heat capacity at all temperatures measured. The heat capacity values thus obtained are C_s under the saturated vapor pressures but the difference between C_s and C_P is negligibly small because the pressures are low and the C_s data are presented as C_P.

Table 4. Smoothed heat capacity values of dinitrogen oxide at rounded temperatures
1 mol N_2O=44.012 8 g, IPTS-68

T/K	C_P/J K^{-1} mol^{-1}	Deviation[a] /%
3	0.019	
5	0.089	
10	0.822	
15	2.918	
20	6.309	+0.16
30	14.40	+0.56
40	21.65	−0.84
50	27.25	+0.13
60	31.47	+0.54
70	34.64	+0.52
80	37.23	+0.62
90	39.41	+0.25
100	41.28	+0.36
110	43.07	+0.28
120	44.86	+0.47
130	46.70	+0.81
140	48.63	+0.86
150	50.70	+0.63
160	52.95	+0.45
170	55.48	+0.32
180	58.28	+0.39
185	77.50	+0.28

a) Deviation=[C_P(Blue and Giauque)−C_P(This)] ×100/C_P(This)

The heat capacity values of dinitrogen oxide without curvature corrections are given in Table 3 and plotted in Fig. 7. The smoothed values at rounded temperatures are given in Table 4, where comparisons are shown with the results by Blue and Giauque[2] in terms of deviations. Blue and Giauque's results are systematically larger than the present results but the differences are probably within the combined limits of errors. A more sensitive comparison can be made by use of equivalent Debye temperature Θ_D, whose temperature dependence for $5N$ degrees of freedom is shown in Fig. 8. We shall discuss the shape of the

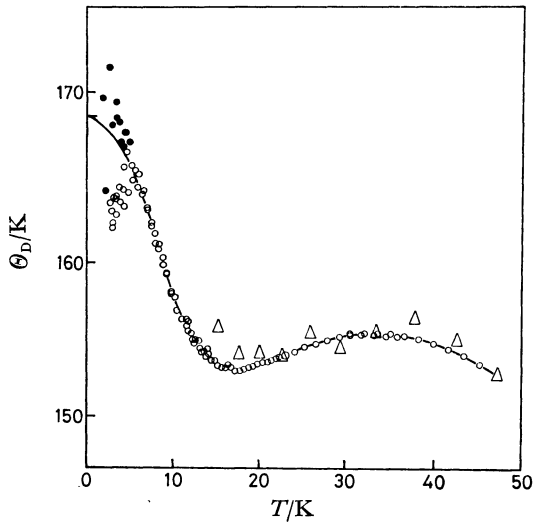

Fig. 8. The Debye characteristic temperatures of dinitrogen oxide derived from the measured heat capacities, assuming $5N$ degrees of freedom. ○, This research (measured with the germanium thermometer α and the platinum thermometer); ●, This research (measured with the germanium thermometer γ); △, R.W. Blue and W.F. Giauque (1935).

Θ_D curve in a later section but here focus our attention on the low temperature end of the curve. Apparently, there is a systematic difference between the results using the germanium thermometer α and those using γ. Since the γ scale is much closer to the measured calibration points than the α scale as is evident from a comparison of Tables 1 and 2, and Figs. 5 and 6, we would place more weight upon the results using the γ thermometer. The results of the two series agree with each other above 3.7 K. The scatter of the present results is much smaller than that of the results by Blue and Giauque: at most ±3% at 4 K, ±1% at 10 K, ±0.1% above 20 K, and ±0.5% above 170 K where the vapor pressure of dinitrogen oxide becomes

Table 5. The heat of fusion of dinitrogen oxide

Amount of sample	Temperature interval	Heat input	(Corrections) $\int C_p dT$	Heat of vaporization	ΔH_f
mol	K	J	J	J	J·mol^{-1}
0.426 5	182.210 0—184.294 6	2 864.77	99.87	4.96	6 511
0.200 7	181.626 9—183.820 8	1 368.43	65.97	12.26	6 521
				average	6 516±20
				Blue and Giauque (1935)	6 541

Table 6. The data of fractional melting of dinitrogen oxide

Fraction melted	Temperature K	Vapor Pressure kPa
0.169	182.404 2	87.96
0.302	182.404 8	87.96
0.435	182.405 2	87.91
0.568	182.405 3	87.91
0.702	182.405 8	87.91
0.835	182.406 0	87.99
(1.000)	(182.406±0.002)	

The triple point of pure dinitrogen oxide: 182.407± 0.002 K. Clusius *et al.* (1930) 182.4 K; Blue and Giauque (1935) 182.26 K.

Table 7. The heat of vaporization of dinitrogen oxide

Starting point (T/K, P/kPa)	Final point (T/K, P/kPa)	Corrected heat input (ΔE/J)	Amount of evaporated N_2O (Δn/mol)
T_1: 184.413 2	T_2: 184.667 3	ΔE:	Δn:
P_1: 99.356	P_2: 100.854	1 096.05	0.065 361 5
T_1: 184.800 3	T_2: 184.816 2	ΔE:	Δn:
P_1: 101.705	P_2: 101.777	1 070.96	0.064 708 0
T_1: 184.674 5	T_2: 184.684 1	ΔE:	Δn:
P_1: 100.925	P_2: 100.947	1 066.27	0.064 493 1

average ΔH_v=16 544±20 J mol^{-1} at 184.81 K

Blue and Giauque (1935)
ΔH_v=16 564±13 J·mol^{-1} at 184.59 K.

significantly high.

Fusion. The curve of the heat capacity of solid dinitrogen oxide shows an upward trend near the triple point (see Fig. 7). However, fusion itself occurs over a narrow range of 0.002 5 K (see Table 6) and therefore the latent heat of fusion was determined in the ususal manner, excluding the premelting portion of the heat capacity. The two series of measurements of heat of fusion are summarized in Table 5 together with the value of Blue and Giauque.[2] The mean value of the heat of fusion of dinitrogen oxide obtained was 6 516±20 J mol^{-1}, which is considerably smaller than the value of Blue and Giauque.[2] The rather large uncertainty in the present value comes from an error in determination of the amount of specimen used in the calorimetry. The triple point temperatures and the amount of impurities were evaluated from fractional melting experiment (see Table 6). The triple point of pure dinitrogen oxide thus determined was 182.407±0.002 K, and the amount of liquid-soluble, solid-insoluble impurities was estimated as 0.001 mol%. The triple point of the dinitrogen oxide used in this calorimetry was 182.406±0.002 K.

Heat of Vaporization. The heat of vaporization of dinitrogen oxide was measured during the second series of calorimetry in the manner as described in the preceding section. The results are summarized in Table 7, showing higher precision than for the heat of fusion because of more precise determination of the amount of the specimen evaporated. The heat of vaporization of dinitrogen oxide was obtained as 16 544±20 J mol^{-1} at 184.81 K and 101.7 kPa, which is again smaller than the value of Blue and Giauque[2] but agrees within the combined limits of error.

Vapor Pressures. The vapor pressures of solid and liquid dinitrogen oxide were measured concurrently with the heat capacity measurements. The results given in Table 8 were fitted to the Antoine equation as follows by the method of least squares;

a) 146 K—182.4 K (triple point): solid

$$\log_{10}(P/\text{Pa}) = -1\,270.42/T + 8.955\,644 - 0.000\,941\,21\,T, \quad (5)$$

b) 182.4 K (triple point)—185 K: liquid

$$\log_{10}(P/\text{Pa}) = -886.293/T + 9.803\,215. \quad (6)$$

Deviations from Eqs. (5) and (6) are also included in Table 8. The normal boiling point of dinitrogen oxide was evaluated as 184.74 K from Eq. (6). From the temperature dependences of vapor pressure described above, the heat of vaporization can be obtained by Clapeyron-Clausius equation: $dP/dT=\Delta H_v/T\Delta V_m$. The results calculated by use of this formula agree with the heat of vaporization determined by calorimetry to within ±0.5%. The molar volume of the gas was evaluated by applying the correction for non-ideality using the second virial data.[10]

Thermodynamic Functions. The thermodynamic functions of dinitrogen oxide were calculated from the smoothed heat capacity values and other data described above and are given in Table 9. The contribution of the heat capacities below the lowest temperature 1.9 K was estimated by a smooth extrapolation, which however was negligibly small.

Table 8. Vapor pressure of dinitrogen oxide

T/K	P/kPa	Deviation $\log_{10}(P_{obsd}/P_{smoothed})$
	(Solid)	
146.071	1.765	0.000 95
149.301	2.698	0.000 10
152.566	4.060	−0.001 37
155.781	5.990	−0.001 32
159.034	8.746	−0.000 71
162.234	12.478	−0.000 90
165.447	17.600	−0.000 59
168.603	24.340	−0.000 54
171.784	33.333	−0.000 53
171.783	33.324	−0.000 60
173.945	40.996	−0.000 49
176.091	50.096	−0.000 41
178.174	60.556	−0.000 44
180.222	72.686	−0.000 25
181.973	84.675	−0.000 11
181.758	83.133	−0.000 06
182.210	86.459	0.000 07
161.506	11.618	0.002 69
165.335	17.488	0.001 76
169.155	25.829	0.001 20
173.105	37.940	0.000 50
173.115	37.958	0.000 31
176.369	51.462	0.000 17
179.489	68.199	0.000 17
181.626	82.243	0.000 22
181.627	82.243	0.000 19
	(Liquid)	
184.295	98.650	−0.000 01
182.405	87.909	−0.000 27
182.408	87.920	−0.000 27
184.875	102.141	−0.000 01
182.617	89.083	−0.000 14
183.813	95.802	−0.000 13
183.822	95.838	−0.000 22
184.660	100.805	−0.000 14
183.577	94.469	−0.000 01
184.410	99.356	−0.000 08
184.413	99.356	−0.000 01
184.667	100.854	−0.000 12
183.821	95.914	0.000 17
182.482	88.500	0.000 60
183.643	94.899	0.000 23
184.679	100.973	0.000 10
184.089	97.475	0.000 14
182.407	87.976	0.000 02
182.407	87.969	0.000 01
183.937	96.548	−0.000 01
183.937	96.553	−0.000 02
184.917	102.419	0.000 09
184.800	101.705	0.000 07
184.816	101.777	−0.000 03
184.674	100.925	−0.000 00
184.684	100.947	−0.000 16

Table 9. Thermodynamic functions of dinitrogen oxide

T/K	$(S°-S_0°)$/J K^{-1} mol^{-1}	$(H°-H_0°)/T$/J K^{-1} mol^{-1}	$-(G°-H_0°)/T$/J K^{-1} mol^{-1}
	(Solid)		
10	0.255 6	0.195 7	0.060
20	2.215	1.669	0.546
30	6.294	4.558	1.736
40	11.467	7.958	3.509
50	16.93	11.28	5.65
60	22.29	14.31	7.98
70	27.39	17.00	10.39
80	32.19	19.37	12.82
90	36.70	21.48	15.22
100	40.95	23.37	17.58
110	44.97	25.08	19.89
120	48.79	26.65	22.14
130	52.46	28.12	24.34
140	55.99	29.52	26.47
150	59.41	30.86	28.55
160	62.76	32.17	30.59
170	66.04	33.46	32.58
180	69.29	34.76	34.53
182.4	70.07	35.08	34.99
	(Liquid)		
182.4	105.79	70.80	34.99
184.8	106.80	70.88	35.92
	(Real gas)		
184.8	196.32	160.40	35.92

Analysis and Discussion

Orientational Disorder. The residual entropy is defined as the difference between the calorimetric and the statistical entropies and represents apparent failure of the third law of thermodynamics. The current interpretation of the residual entropy is based on one of three possibilities; (1) anomaly in the heat capacity exists below the lowest measured temperature, (2) degeneracies of the spin-rotation interaction are partially removed in the crystal lattice, and (3) the solid is in non-equilibrium state which is frozen-in at the lowest temperature attained.

Since Giauque *et al.*[1,2] reported the existence of residual entropy in carbon monoxide and dinitrogen oxide and presented an interpretation that the entropy arose from head-to-tail disorder of molecular arrangement, a number of papers were published to identify its origin with either (1) or (3). Thus, Melhuish and Scott[3] calculated electrostatic energies of some molecular crystals and suggested that the Curie temperatures for dipole orientation in CO and N_2O would be 5 and 11 K, respectively. Because these temperatures were lower than 15 K from which Giauque *et al.*[1,2] started heat capacity measurements, attempts were made to extend the measurements on CO to lower temperatures.[4,5] The results were, however, inconclusive; no additional phase transition was observed down to 2.5 K. Later experiments by Burford and Graham[7] went as far down as 0.8 K without detecting any anomalies either. Although there still remains a

possibility that the experimental temperatures were not low enough to see the removal of the residual entropy, odds are in favor of the 'freezing-in' interpretation. In the mean time, Pitzer *et al.*[6] considered the kinetics of the order-disorder transition in solid carbon monoxide by a tunneling mechanism and showed that the rate of transition was too small to produce a heat capacity anomaly.

The situation is quite analogous in the case of dinitrogen oxide which has a very small dipole moment of 0.55×10^{-30} Cm and the same crystal structure as the low-temperature form of carbon monoxide. Because the calculated Curie temperature of dinitrogen oxide was higher by a factor of 2, a greater chance was to be expected to observe a heat capacity anomaly. However, the experimental heat capacity curve is quite normal down to 1.9 K as shown in Fig. 7 and in the following section. We consider that this is due to 'freezing-in' of the end-for-end reorientational motion below the triple point partly because the potential barrier hindering such motion may be as high as 4000 K, as estimated from the libration frequency of 70 cm^{-1}, and partly because it would be hardly conceivable to be unable to find a rotational transition down to 1.9 K if we were dealing with the perfect equilibrium state.

TABLE 10. THE ENTROPY OF DINITROGEN OXIDE.

Contribution	$S°$/J K^{-1} mol^{-1}
The calorimetric entropy	
0K——2K (smooth extrapolation)	0.002
2K——182.41K (graphical)	70.07
Fusion (6 516/182.41)	35.72
182.41 K——184.81 K (graphical)	1.01
Vaporization (16 544/184.81)	89.52
The entropy of actual gas at 184.81 K	196.32±1.0
The entropy of ideal gas at 184.74 K	196.8 ±1.0
The statistical entropy	
S (trans.)	145.99
S (rot.)	55.87
S (vib.)	0.96
The statistical entropy at 184.74 K	202.8
The residual entropy	6.0 ±1.0
Blue and Giauque (1935)	$S_0°$=4.8

The residual entropy of dinitrogen oxide was re-evaluated by using the present calorimetric results and recent molecular constants. The details of calculation is given in Table 10 which gives $S_0=6.0\pm1.0$ J K^{-1} mol^{-1}, very close to $R\ln2=5.76$ J K^{-1} mol^{-1}. Therefore, it appears that molecular reorientation has become frozen somewhere between the triple point and 1.9 K but exactly where it occurs is not known. The measurements of heat capacity were carried out quite normally: Nowhere slow equilibration phenomenon was observed as was in the case of ice.[14]

Lattice Frequency Spectrum. Very little is known about the lattice frequency spectrum of molecular crystals having internal degrees of freedom. Simple ionic crystals (*e.g.* NaCl), covalent crystals (*e.g.* Ge), metals and other monatomic crystals (*e.g.* Ar) have been studied and the shape of their frequency spectra is rather well known. Molecular crystals may be characterized by small force constants for intermolecular interaction, compared with other types of solids. Such characteristics should manifest themselves in the vibrational spectrum of the solids. We shall examine this by an analysis of the low-temperature heat capacities through Debye temperature cruve and moments of lattice frequency spectrum of N_2O.

The Debye temperature curve converted from the measured heat capacity values for $5N$ degrees of freedom is given in Fig. 8. Very shallow, broad minimum is a feature of molecular crystals in contrast to the cases of ionic and covalent crystals. The feature should more clearly be seen by deriving the even moments $\mu_n(\nu)$ of the lattice vibration spectrum. To do this, contributions from translational modes of vibration were extracted from measured heat capacity values by subtracting intramolecular and libration contributions. Here we used frequency values 1 293, 590, and 2 240 cm^{-1} for intramolecular vibrations and 70 (E), 83 (T), and 126 cm^{-1} (T) for librations. The C_p–C_v corrections were negligibly small below 25 K. The procedure for calculating the moments were the same as in the previous paper.[8] Moments of different order n may be compared by deriving $\nu_D(n)$,

$$\nu_D(n)=\left[\frac{1}{3}(n+3)\mu_n\right]^{1/n} \quad (n>-3). \tag{7}$$

This is plotted as a function of n in Fig. 9. Points have also been included in Fig. 9 that correspond to $\nu_D(-3)$ (from $\Theta_0=141.0\pm1.0$ K), $\nu_D(0)$ (from $\Theta_\infty{}^S=141$ K), and $\nu_D(1)$ (from E_z; see following subsection). The ν_D functions for other values of n were not obtained because of poor convergence of expansion formulae. Figure 9 shows that there is a flat region for low n where there is a deep minimum in the case of NaCl or other strongly ionic crystals. This is the portion where contributions from low-frequency end of the spectrum are the largest. A difference in vibrational properties between ionic (covalent) and molecular crystals lies, therefore, in the fact that vibrational modes are more condensed into the low-frequency portion of the spectrum in molecular crystals.

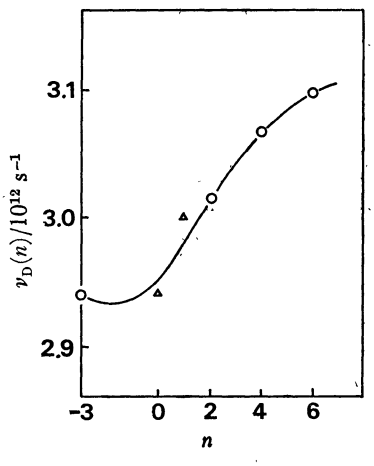

Fig. 9. Plot of $\nu_D(n)$ against n for solid dinitrogen oxide. △, from approximate calculation (see in text).

Zero-point Properties. Some of the properties of solid N_2O at 0 K will be summarized here.

Θ_0 was obtained from a plot of C/T^3 *vs.* T^2 as 141.0 ± 1.0 K for $3N$ degrees of freedom. If one uses 'translational' heat capacity curve for $5N$ degrees of freedom, Θ_0 becomes 167.4 ± 1.0 K.

Static lattice energy was derived by analysis of the vapor pressure data which were fitted to the formula[15]

$$\ln(PT^{3/2}) = (a/T) + b. \quad (8)$$

The static lattice energy E_0 is related to a through

$$aNk = E_0' = E_0 - E_{z,\mathrm{lib}}, \quad (9)$$

where $E_{z,\mathrm{lib}}$ is the zero-point librational energy. The slope of a graph of $\ln(PT^{3/2})$ against T^{-1} gives E_0' a value of 25.91 kJ mol^{-1}. A small correction to this value must be made for the effect of defect formation in the neighborhood of the triple point,[15] which leads to a revised value of 26.0 kJ mol^{-1}. $E_{z,\mathrm{lib}}$ can be evaluated approximately from the librational frequencies as 1.15 kJ mol^{-1}; therefore $E_0=27.2$ kJ mol^{-1}.

The total zero-point energy E_z may be obtained as the difference between the static lattice energy E_0 and the heat of sublimation at 0 K which is 24.21 kJ mol^{-1}. Thus, $E_z=3.0$ kJ mol^{-1} of which 1.85 kJ mol^{-1} is the translational zero-point energy $E_{z,\mathrm{trans}}$. $E_{z,\mathrm{trans}}$ can also be obtained from $\nu_D(1)$. By smooth interpolation of Fig. 10, one obtains $E_{z,\mathrm{trans}}=1.34$ kJ mol^{-1} which is some 0.5 kJ mol^{-1} smaller but is in reasonable agreement with the value derived from E_0 and $\Delta H_v°$. The discrepancy probably comes from the uncertainty in the value of E_0.

Premelting Phenomenon. As is evident from Fig. 7, the heat capacity of solid N_2O tends to increase with a positive curvature from about 120 K to the triple point. We may call this phenomenon 'premelting' although it does not actually correspond to liquid formation. Similar tendency has been noted in a number of low-melting metals and some molecular crystals. It has been customary to account for the effect in terms of formation of vacancies in the crystalline lattice.

Other possibilities such as anharmonicity of the lattice vibration cannot be ruled out in general; but this is rather unlikely for the following reasons. Taking solid argon as an example, the anharmonicity, if any, appears in such a way that the heat capacity increases to a smaller extent than expected for a Debye solid, *i.e.*, the Debye temperature becomes gradually higher as the temperature is increased from about 40 K.[16] This means that the resultant heat capacity curve should never show a positive curvature after it has passed the Θ_D minimum. Moreover, the volume expansivity of argon shows the same trend as the heat capacity below the triple point. In the case of dinitrogen oxide, contributions from librational freedom of motion makes a similar analysis of the Θ_D curve much less meaningful but nevertheless it is quite reasonable to assume that some kind of defect formation is progressively excited as the triple point is approached.

Now by assuming that separated lattice imperfections are thermally created and their equilibrium concentration is determined by the Boltzmann factor, one obtains an excess ΔC_p of the heat capacity

$$\Delta C_p = \frac{\Delta H_s^2}{RT^2} \exp(\Delta S_s/R) \exp(-\Delta H_s/RT), \quad (10)$$

and the enthalpy of defect formation ΔH_s derived from a plot of $\log(T^2\Delta C_p)$ *vs.* $1/T$. The excess heat capacity was estimated by taking differences between the observed and the 'normal' heat capacity; the latter was obtained by smooth extrapolation from about 50 K upwards. The value of ΔH_s thus obtained is 10.8 ± 0.6 kJ mol^{-1}, corresponding to 45% of the heat of sublimation 24.2 kJ mol^{-1} at 0 K.

There is no direct experimental evidence that enables us to fix the type of imperfections. The equilibrium concentration of the imperfection at the triple point is only 2%; therefore very precise diffraction methods would only help to elucidate the nature of imperfections. The only clue we have at present is the magnitude of ΔH_s and its comparison with other relevant properties.

It is interesting to compare N_2O with iso-structural α-N_2 and α-CO. The low-temperature α-phase of nitrogen has an approximate space group Pa3 ($P2_13$ to be exact) and the α-phase of CO is also of Pa3. In this structure, the molecular centers are arranged at the lattice points of the fcc unit cell and the molecules are directed toward one of four equivalent body diagonals of the cell. By X-ray and nuclear quadrupole resonance studies of the high-temperature β-phase of N_2 (hexagonal), the molecules were shown to precess about the c-axis with an angle of precession 55°. This precession angle is exactly equal to the angle which a molecule makes with the c-axis in the α-phase. To visualize the mechanism of the phase transition at 35.61 K in N_2, the molecules undergo a precessional oscillation about the crystallographic axes and, as the temperature is increased, some molecules reorient themselves into another body-diagonal direction. In connection with such a phase transition, the heat capacity of nitrogen also shows an upward curvature below the transition point besides the similar phenomenon observed below the triple point.[17] An interpretation of the low-temperature tail of the transition is one by what might be called 'orientational defect', *i.e.*, some molecules are disoriented from their normal direction or some undergo reorientational motion. Application of Eq. (10) to the excess heat capacity of N_2 below its transition point leads to a value of 2 kJ mol^{-1} for the enthalpy of formation of an orientational defect. This value is not accurate because the heat capacity measurements were not closely spaced. However analogous treatment for the case of CO, for which more appropriate data are available,[4,5] gives $\Delta H_s=3$ kJ mol^{-1} or 38% of the heat of sublimation at 0 K.

We would thus like to propose that the pre-melting excess of heat capacity in N_2O mainly arises from thermal creation of orientational defects with the enthalpy of formation 10.8 kJ mol^{-1}. It is very likely that 'positional' defects or vacancies are also present at the same time, which probably accompany a heat effect of some 16 kJ mol^{-1} or more and are not seen in the present analysis.

For diatomic and pseudo-diatomic molecules, N_2, CO, and C_2H_2, the transition temperature T_c is determined by quadrupole interaction as inferred from close correla-

tion between T_c and Θ^2/R^5 where Θ is the molecular quadrupole moment and R is the nearest neighbor distance. In the case of triatomic molecules, N_2O and CO_2, repulsive interaction is so large as to push T_c to above the triple point but not too far above, because orientational disorder is in fact a pre-transition effect.

References

1) J. O. Clayton and W. F. Giauque, *J. Amer. Chem. Soc.*, **54**, 2610 (1932).
2) R. W. Blue and W. F. Giauque, *ibid.*, **57**, 991 (1935).
3) M. W. Melhuish and R. L. Scott, *J. Phys. Chem.*, **68**, 2301 (1964).
4) T. Shinoda, T. Atake, H. Chihara, Y. Mashiko, and S. Seki, *Kogyo Kagaku Zasshi*, **69**, 1619 (1966).
5) E. K. Gill and J. A. Morrison, *J. Chem. Phys.*, **45**, 1585 (1966).
6) R. F. Curl, Jr., H. P. Hopkins, Jr., and K. S. Pitzer, *ibid.*, **48**, 4064 (1968).
7) J. C. Burford and G. M. Graham, *Can. J. Phys.*, **47**, 23 (1969).
8) T. Atake and H. Chihara, *J. Chem. Thermodynamics*, **3**, 51 (1971).
9) T. Shinoda, H. Chihara, and S. Seki, *J. Phys. Soc. Japan*, **19**, 1637 (1964).
10) H. L. Johnston and H. R. Weimer, *J. Amer. Chem. Soc.*, **56**, 625 (1934).
11) W. Heuse, *Z. Phys. Chem.*, **A147**, 266 (1930).
12) L. Vegard, *Z. Phys.*, **71**, 465 (1931).
13) A. J. Leadbetter, D. J. Taylor, and B. Vincent, *Can. J. Chem.*, **42**, 2930 (1964).
14) a) O. Haida, T. Matsuo, H. Suga, and S. Seki, *Proc. Japan Acad.*, **48**, 489 (1972); b) O. Haida, H. Suga, and S. Seki, *ibid.*, **49**, 191 (1973).
15) a) L. S. Salter, *Trans. Faraday Soc.*, **59**, 657 (1963); b) H. Chihara and N. Nakamura, This Bulletin, **41**, 1787 (1968).
16) R. H. Beaumont, H. Chihara, and J. A. Morrison, *Proc. Phys. Soc.*, **78**, 1462 (1961).
17) W. F. Giauque and J. O. Clayton, *J. Amer. Chem. Soc.*, **55**, 4875 (1933).